Brain Stimulation 17 (2024) 1048–1059

Contents lists available at ScienceDirect

Brain Stimulation

journal homepage: www.journals.elsevier.com/brain-stimulation

Focused magnetic stimulation for motor recovery after stroke

Ja-Hae Kim [a,1], Minhee Jeong [b,1], Hohyeon Kim [c,1], Ji-Hye Kim [d], Ji Woong Ahn [e], Boyoung Son [c], Kang-Ho Choi [d,*], Seungsoo Chung [b,e,**], Jungwon Yoon [c,***]

[a] Department of Nuclear Medicine, Chonnam National University Medical School and Hospital, Gwangju, South Korea
[b] Department of Physiology, Graduate School of Medical Science, Brain Korea 21 Project, Yonsei University College of Medicine, Seoul, South Korea
[c] School of Integrated Technology, Gwangju Institute of Science and Technology, Gwangju, South Korea
[d] Department of Neurology, Chonnam National University Medical School and Hospital, Gwangju, South Korea
[e] BnH Research Co., LTD., Goyang-si, Gyeonggi-do, South Korea

ARTICLE INFO

Keywords:
Magnetic
Stimulation
Stroke
Nanoparticle
Hyperexcitability

ABSTRACT

Background and objectives: The effects of noninvasive focused magnetothermal brain stimulation using magnetic nanoparticles (MNPs) on post-stroke motor deficits and metabolic dormancy in subacute ischemic injury are not well-established. This study examined if magnetothermal brain stimulation using magnetic nanoparticles (Nano-MS) enhances motor recovery after stroke.

Methods: We randomly distributed rats into Sham, Control, MNP injection only, and Nano-MS groups. We administered focused magnetic stimulation for 30 min daily following an MNP injection (15 mg/mL) into the targeted motor cortex via the carotid artery three weeks after the transient (90 min) middle cerebral artery occlusion. We assessed motor functionality via behavioral tests and conducted positron emission tomography (PET) imaging to verify cerebral metabolic activity. We assessed neuronal excitability, neuroinflammation, blood-brain barrier (BBB) integrity, and neurogenesis four weeks post-stroke.

Results: The Nano-MS group exhibited significantly improved motor deficits and cerebral metabolic activity compared to the Control and MNP groups ($p < 0.05$). Focused Nano-MS modulated neuronal excitability, evident by a depolarized action potential threshold for spike initiation and reduced firing frequency post-stroke. The Nano-MS group demonstrated markedly decreased inflammatory markers, such as IL-1β, IL-6, TNF-α, MCP-1, and ICAM-1, compared to the Control and MNP groups. BBB integrity and immunofluorescence for neurogenesis markers were substantially improved in the Nano-MS group.

Conclusions: Focused Nano-MS facilitates the recovery of motor deficits and metabolic inactivity in the brain by effectively modulating excitability, reducing neuroinflammation, enhancing BBB stability, and promoting neurogenesis. Nano-MS is a potential novel, noninvasive therapy for stroke rehabilitation. Further investigation is warranted.

1. Introduction

Stroke remains the leading cause of severe chronic functional disability worldwide. The insufficient recovery of walking ability in the chronic post-stroke phase is a particularly challenging consequence [1]. Most survivors exhibit significant residual motor weakness despite comprehensive contemporary rehabilitation efforts. There is growing interest in developing innovative neurostimulation treatments to enhance post-stroke motor recovery [2–4]. Unlike invasive techniques, noninvasive alternatives, such as repetitive transcranial magnetic stimulation (rTMS) and transcranial direct current stimulation (tDCS), are more practical and may offer lasting, demand-based control effects [4].

* Corresponding author. Department of Neurology, Chonnam National University Medical School and Hospital, 42 Jebongro, Donggu, Gwangju, 61469, South Korea.
** Corresponding author. Department of Physiology, Graduate School of Medical Science, Brain Korea 21 Project, Yonsei University College of Medicine, Seoul, 03722, South Korea.
*** Corresponding author. School of Integrated Technology, Gwangju Institute of Science and Technology, Gwangju, South Korea.
E-mail addresses: ckhchoikang@hanmail.net, ckhchoikang@chonnam.ac.kr (K.-H. Choi), sschung@yuhs.ac (S. Chung), jyoon@gist.ac.kr (J. Yoon).
[1] These authors contributed equally to the manuscript.

https://doi.org/10.1016/j.brs.2024.08.011
Received 13 February 2024; Received in revised form 22 August 2024; Accepted 27 August 2024
Available online 28 August 2024

Ischemic stroke can induce neuronal excitability in the affected hemispheres, which is associated with post-stroke motor disability [5,6]. Current noninvasive brain stimulation methods under clinical investigation show improvements in motor recovery after stroke by modulating abnormal brain excitability [2,3,7–9]. Although rTMS or tDCS can indirectly stimulate deep brain regions by targeting superficial brain structures such as the cortex, they cannot directly penetrate the brain and lack precise localization of the target brain region [4] Therefore, innovative, noninvasive brain stimulation methods are required. We have recently demonstrated that focused magnetothermal brain stimulation using magnetic nanoparticles (MNP) significantly elevates the temperature of precisely localized target brain regions, facilitating stimulation. Moreover, our prior proof-of-concept study showed that focused magnetothermal stimulation using MNP (Nano-MS) accesses deep brain targets [10].

Excitation of MNPs by a low radiofrequency field of magnetic stimulation can release energy as heat to surrounding tissues and increase the temperature without perturbing brain cells [11]. MNPs are injected systemically and stick to the blood vessel wall due to the non-zero gradient magnetic field in the field-free point (FFP) region. Focused magnetic stimulation can be applied to the targeted region, providing thermal stimulation to only that area. However, the concrete effect and the detailed therapeutic mechanism of focused Nano-MS treatment remain unclear.

In this study, we present the effects of focused Nano-MS on modulating the excitability of the primary motor cortex, aiming to enhance motor recovery and cerebral metabolic function post-ischemic stroke. Furthermore, we explored the therapeutic mechanism of focused Nano-MS in post-stroke motor rehabilitation, examining its effects on neuroinflammation, blood-brain barrier (BBB) integrity, apoptosis, and neurogenesis.

2. Materials and methods

2.1. Animals

All animal protocols adhered to the Chonnam National University guidelines for the care and use of laboratory animals and received approval from the Institutional Animal Care and Use Committee (IACUC). The study complied with the National Institutes of Health (NIH) guidelines concerning the care and use of animals in experimental procedures. The animals were kept on a 12-h light/dark cycle with ad libitum access to food and water. We obtained adult (8-week-old) male Sprague-Dawley (SD) rats, with body weights of 250–290 g, from Samtako Bio Korea

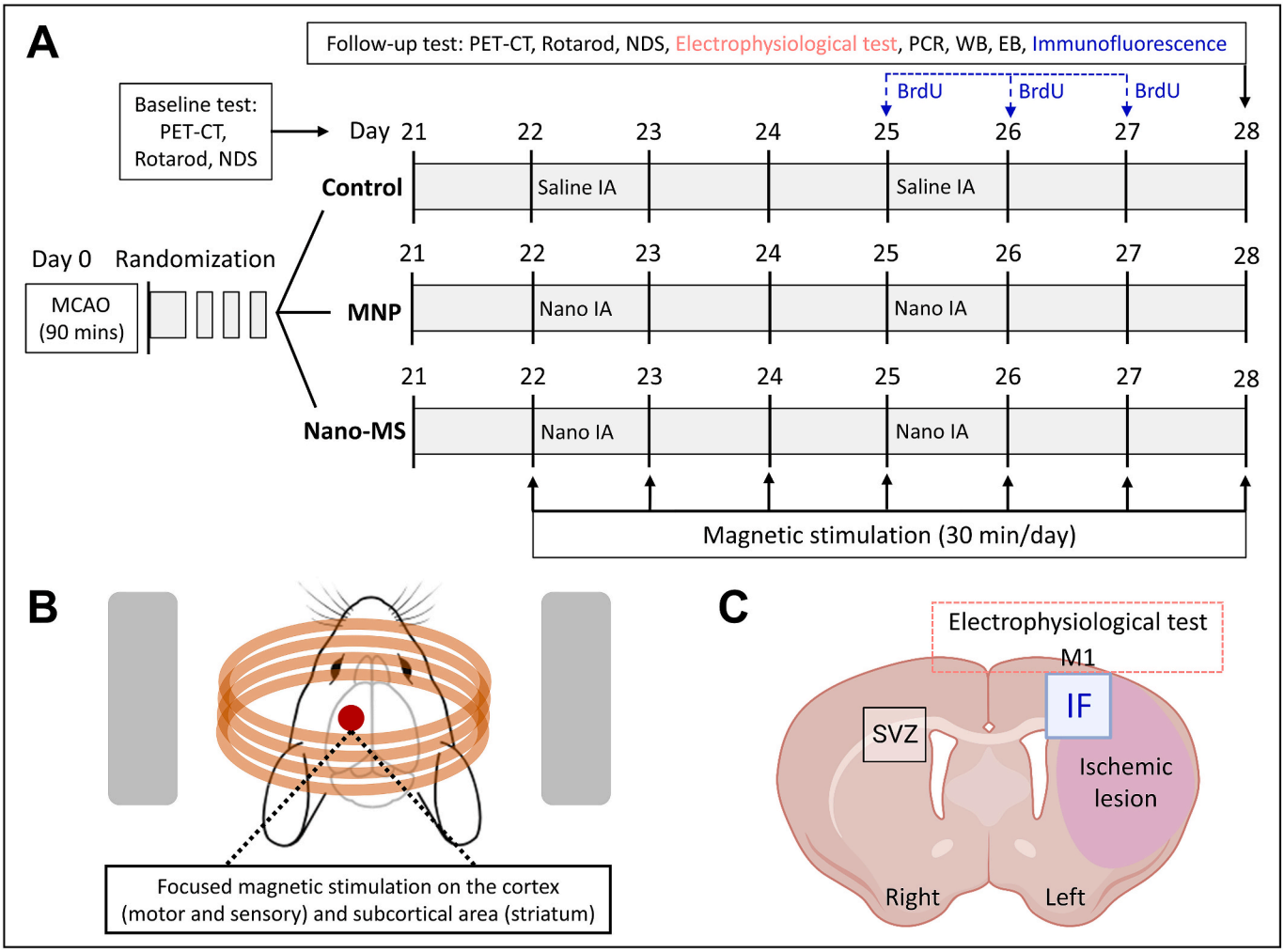

Fig. 1. Experimental arrangement. (A) We introduced magnetic nanoparticles at a concentration of 15 mg/mL via the carotid artery, followed by 30 min of daily magnetic stimulation to the target brain area for one week. (B) The magnetic stimulation was directed at the motor and sensory cortex and the subcortical striatum. (C) We performed electrophysiology studies and immunofluorescence (IF) staining on the border region of the frontal cortex adjacent to the subventricular zone (SVZ).

NDS = Neurological deficit score; EB = Evans blue; MCAO = Middle cerebral artery occlusion; IA = Intra-arterial injection; SVZ = Subventricular zone; IF = Immunofluorescence. (For interpretation of the references to colour in this figure legend, the reader is referred to the Web version of this article.)

Co., Ltd. (Seoul, Korea). Local authorities sanctioned the animal procedures in accordance with national regulations on animal care.

2.2. Surgical procedures

To create the middle cerebral artery occlusion (MCAO) model, we occluded the left middle cerebral artery (MCA) for 90 min in SD rats using the intraluminal filament method as previously described [12]. Three weeks after the MCAO, we administered magnetic nanoparticles (MNP) via the ipsilateral carotid artery at a concentration of 15 mg/mL (total volume 60ul). This injection was immediately followed by 30 min of magnetic stimulation of the rat brains. This regimen was repeated for one week, with daily magnetic stimulation and biweekly MNP administrations at three-day intervals (Fig. 1A). We randomly distributed the animals into four treatment groups. The first experimental group underwent sham surgery without MCAO (Sham group). The second group received saline post-MCAO (Control group). The third group was administered MNP post-MCAO (MNP group). The fourth group underwent daily 30-min magnetic stimulation following MNP administration post-MCAO (Nano-MS group). Detailed methodical descriptions are provided in the Supplementary Materials.

2.3. Focused magnetic stimulation

We utilized Synomag-D, a commercially available particle, as the heat transfer medium. We determined the particle's specific loss of power (SLP) as 139 W/g, based on the experimentally measured temperature [13]. The characterized MNPs experience magnetic relaxation in the FFP region. This is generated by the superposition of an alternating magnetic field with 7 mTrms at 595.4 kHz from a 17-turn coil with a diameter of 5 cm and a gradient magnetic field of 2.1 T/m from a pair of permanent magnets. This combined magnetic field induces the MNPs to generate heat. The generated FFP allows the thermal energy to be focused on a specific target area. We validated the target heating efficiency range and the MNP's heating efficiency via COMSOL simulation for the measured SLP (**eFigure I**) [14]. Detailed methodical descriptions are provided in the Supplementary Materials.

2.4. Behavioral tests

We performed a neurological examination at defined intervals following MCAO in all rats except for the sham group. An investigator blinded to the experimental groups evaluated the neurological deficit score (NDS) [15]. Only rats with a pre-treatment NDS score of 1 were included in the study. Motor function was assessed through the accelerating rotarod test. Each experimental group underwent a 5-min pre-training two to three times before the initial treatment and after the final one. The rotarod was steadily accelerated over 5 min, and we measured how long (in seconds) the rat remained on the rotating drum until it fell. Each session encompassed three successive attempts with a cap of 300 s at 10 RPM. We derived the average of three attempts for behavioral tests.

2.5. Brain PET imaging

We acquired PET brain images twice using a preclinical PET-CT scanner: initially at baseline and subsequently following Nano-MS. Rats without stroke lesions in the baseline PET-CT images were excluded from the study. We analyzed the PET brain images using PMOD. We calculated the glucose uptake (%ID/g) to compare the PET signal intensity values from the first and second scans for each rat. We generated subtraction images to visualize the changes between the two PET scans post-treatment. The difference between the scans was expressed as the uptake ratio (%), calculated using the formula: [(mean of the second scan-mean of the first scan)/mean of the first scan] × 100. Detailed methodologies are described in the Supplementary Materials.

2.6. Electrophysiology

We obtained whole-cell patch clamp recordings from pyramidal neurons in the second and third layers of the motor cortex (M1) (Fig. 1C). Recordings were confined to the motor cortical area defined by the stereotaxic coordinates [16]. To establish the relationship between injected current amplitude and firing frequency (*f*-I curve), we counted the number of action potentials (APs) induced by 500-ms depolarizing current pulses ranging from 0 to 400 pA in 50 pA steps occurring in 500 ms and then converted them into firing frequency (Hz). The rheobase was defined as the amplitude of the minimum current step to elicit at least a single AP. Input resistance was characterized as the linear slope of the relationship between hyperpolarizing current from −100 pA to 0 pA in 50 pA increments and the average membrane potential for the entire length of the current step [17]. AP threshold, afterhyperpolarization (AHP) amplitude, AHP duration, and AHP slope were characterized in a voltage trace elicited by a current pulse of 300 pA [18]. Detailed methodologies are described in the Supplementary Materials.

2.7. Immunoblot analysis and quantitative reverse transcription polymerase chain reaction (qRT-PCR)

We bisected the brains of MCAO rats to segregate their left (ischemic) hemispheres (n = 6 for each group). We prepared protein extracts to evaluate the expression patterns of occludin, JAM-A, claudin-5, zona occludens-1 (ZO-1), matrix metalloproteinase-9 (MMP-9), and β-actin in the ischemic hemispheres. To quantify of the protein expression levels, we calculated the mean gray value for each band using Image J software.

We extracted total RNA from the brain tissues and subsequently synthesized cDNA. We conducted RT-PCR assays in duplicate for tumor necrosis factor-alpha (TNF-α), ionized calcium-binding adaptor molecule 1 (Iba-1), interleukin-1 beta (IL-1β), interleukin-6 (IL-6), monocyte chemoattractant protein-1 (MCP-1), and intercellular adhesion molecule-1 (ICAM-1). Glyceraldehyde-3-phosphate dehydrogenase (GAPDH) was a reference gene as an internal control for the qRT-PCR analysis. The detailed methodology is detailed in the Supplementary Materials.

2.8. Immunofluorescence and fluorescence imaging

To assess whether Nano-MS can activate neurons in the primary motor cortex, we performed double labeling immunofluorescence with c-fos and NeuN in normal rats. We quantified the proportion of c-fos positive neurons in the primary motor cortex. For the c-fos staining experiments, we sacrificed the rats 90 min after a single 30-min magnetic stimulation followed by MNP administration in the Nano-MS group. As a previously demonstrated method to permeate the brain, we intraperitoneally administered BCTC (30 mg/kg, MedChemExpress), a CNS penetrant transient receptor potential (TRP) vanilloid-1 (TRPV1) antagonist, before the Nano-MS manipulation in the Nano-MS + BCTC group [19]. The thymidine analog 5-bromo-2′-deoxyuridine (BrdU; Sigma-Aldrich, St Louis, MO, USA) was used to label proliferating cells. We injected the solution intraperitoneally at 50 mg/kg (10 mg/mL) into each group. For the final three days, we administered BrdU to maximize proliferating cell labeling (Fig. 1).

To assess neurogenesis levels, we performed double labeling with fluorescent-tagged secondary antibodies. We washed the sections with buffer and incubated them with primary antibodies against doublecortin (DCX) to detect neuronal progenitor cells, NeuN for mature neurons, or cleaved caspase-3 (CC3) as an apoptosis marker at four weeks. We prepared six slices from six rats for each group. At 200x magnifications, we counted double-labeled cells in the prespecified boundary area of the frontal cortex adjacent to the subventricular zone in each brain to ensure identical quantified methods (Fig. 1C). We utilized Evans blue staining and an in vivo imaging system (IVIS lumina S5, PerkinElmer) to

investigate magnetic heating-induced changes in BBB permeability and assess the safety of Nano-MS [10]. Detailed methodological descriptions are provided in Supplementary Materials.

2.9. Statistical analysis

The sample size of each experiment was chosen empirically to provide sufficient statistical power to detect the treatment effects. According to a two-tailed calculation, type I error of 0.05, and power of 0.9, the sample size was six rats per group to clarify the brain metabolism using PET-CT and motor function using the rotarod test based on our prior proof-of-concept study. The normality of data distribution was evaluated using the Shapiro–Wilk test, and the homogeneity of variance between groups was assessed with Levene's test. Parametric data were analyzed using one-way ANOVA with Tukey's multiple comparison tests and presented as mean ± standard deviation or standard error of the mean. For data with unequal variances, ANOVA with Welch's correction was employed, followed by Dunnett's multiple comparisons. Nonparametric data were analyzed with the Kruskal–Wallis test followed by Dunn's post hoc analysis and were presented as median [interquartile range]. Parametric tests were applied to data with a small sample size ($n < 6$) [20]. The rotarod test, which involved repeated trials, was assessed for sphericity using Mauchly's test. When the sphericity assumption was violated, Greenhouse–Geisser estimates were used for correction. After confirming the assumption of equality of covariance between groups, the rotarod test data were analyzed using repeated-measures ANOVA to determine the interaction effect between treatment and time (treatment × time), as well as the main effects of experimental treatment and time, followed by Tukey's post hoc test. A probability value (P) < 0.05 was considered statistically significant, with * indicating $p < 0.05$, ** indicating $p < 0.01$, and *** indicating $p < 0.001$. All measurements were taken by observers who were blinded to the individual treatments.

3. Results

3.1. Nano-MS induces neuronal activation by TRPV1 channels

To investigate whether Nano-MS can induce neuronal activation, we performed c-fos and NeuN double immunofluorescence staining in the primary motor cortex after Nano-MS (Fig. 2). The Nano-MS group exhibited a significantly larger proportion of c-fos positive neurons compared to the naïve group (naïve: 0.71 ± 0.45 %; Nano-MS: 41.05 ± 15.46 %, ANOVA with Tukey's post hoc analysis, corrected $p = 0.008$; **eTable I**). To clarify the involvement of TRPV1, a thermo-sensitive channel, in neuronal activation via Nano-MS, we administrated BCTC, a CNS penetrant TRPV1 antagonist, before the Nano-MS manipulation. The administration of the TRPV1 antagonist markedly reduced c-fos positive neurons compared to the Nano-MS group (Nano-MS + BCTC: 3.71 ± 1.39 %; corrected $p = 0.023$; **eTable I**).

3.2. Brain PET imaging

We utilized ^{18}F-FDG PET to evaluate the alterations in metabolic activity pre- and post-treatment. Baseline infarct volumes were similar between the groups (**eTable II**). Relative to baseline, the metabolic function of the brain in both the Control and MNP groups remained comparable after a one-week treatment period (Fig. 3). However, an analysis of the data before and after Nano-MS therapy indicated a marked elevation in metabolic activity within the focused stimulated cortex (22.4 %) and the subcortex (21.7 %). Brain metabolic function was significantly restored following focused stimulation in the Nano-MS group compared to baseline (pre-Nano-MS therapy vs. post-Nano-MS therapy; $p < 0.05$). The increase in glucose metabolism uptake ratio was notably greater in the Nano-MS group than in the Control and MNP groups ($p < 0.001$; **eTable II**).

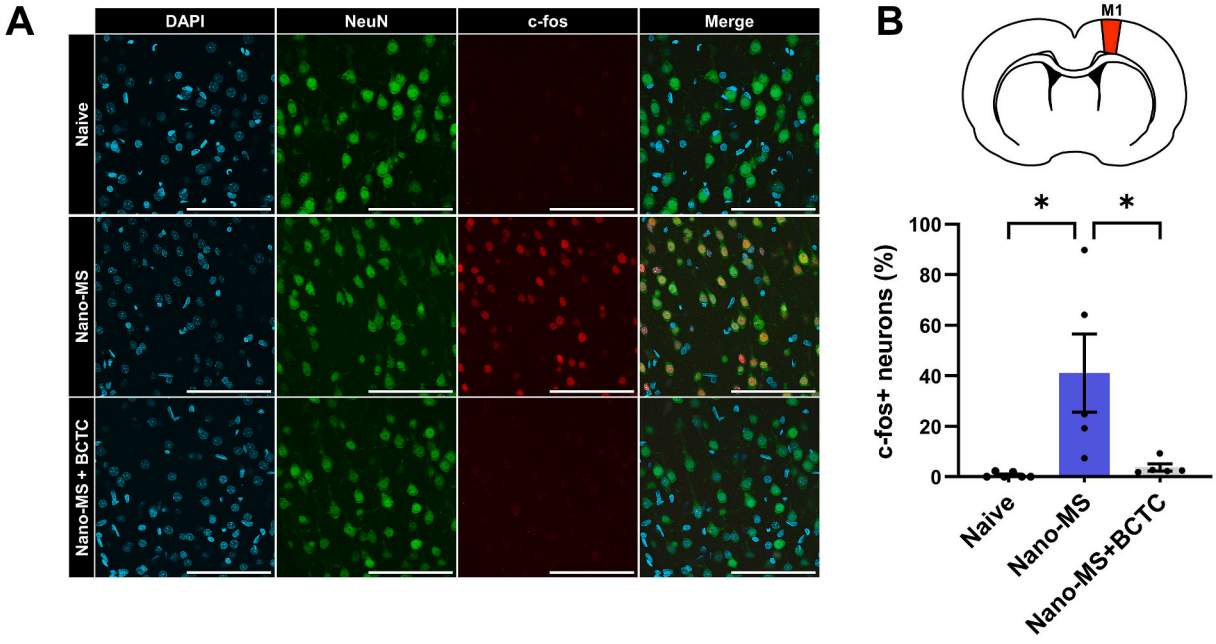

Fig. 2. c-fos immunofluorescence images in the primary motor cortex. (A) Representative fluorescence images of DAPI (cyan), NeuN (green), and c-fos (red) stained brain slices in the primary motor cortex in the naïve, Nano-MS, and Nano-MS pre-treated with TRPV1 antagonist BCTC groups (scale bar = 100 μm). (B) Group average of the proportion of c-fos positive neurons for each group (naïve: 0.71 ± 0.45; Nano-MS: 41.05 ± 15.46; Nano-MS + BCTC: 3.71 ± 1.39, one-way ANOVA, $p = 0.008$). We quantified three fields of view in a single brain slice per animal. The data are shown as the mean ± standard error of the mean (n = 6, 5, and 5 for Naïve, Nano-MS, and Nano-MS + BCTC, respectively). *: $p < 0.05$. We performed a statistical comparison using one-way ANOVA with Tukey tests. (For interpretation of the references to colour in this figure legend, the reader is referred to the Web version of this article.)

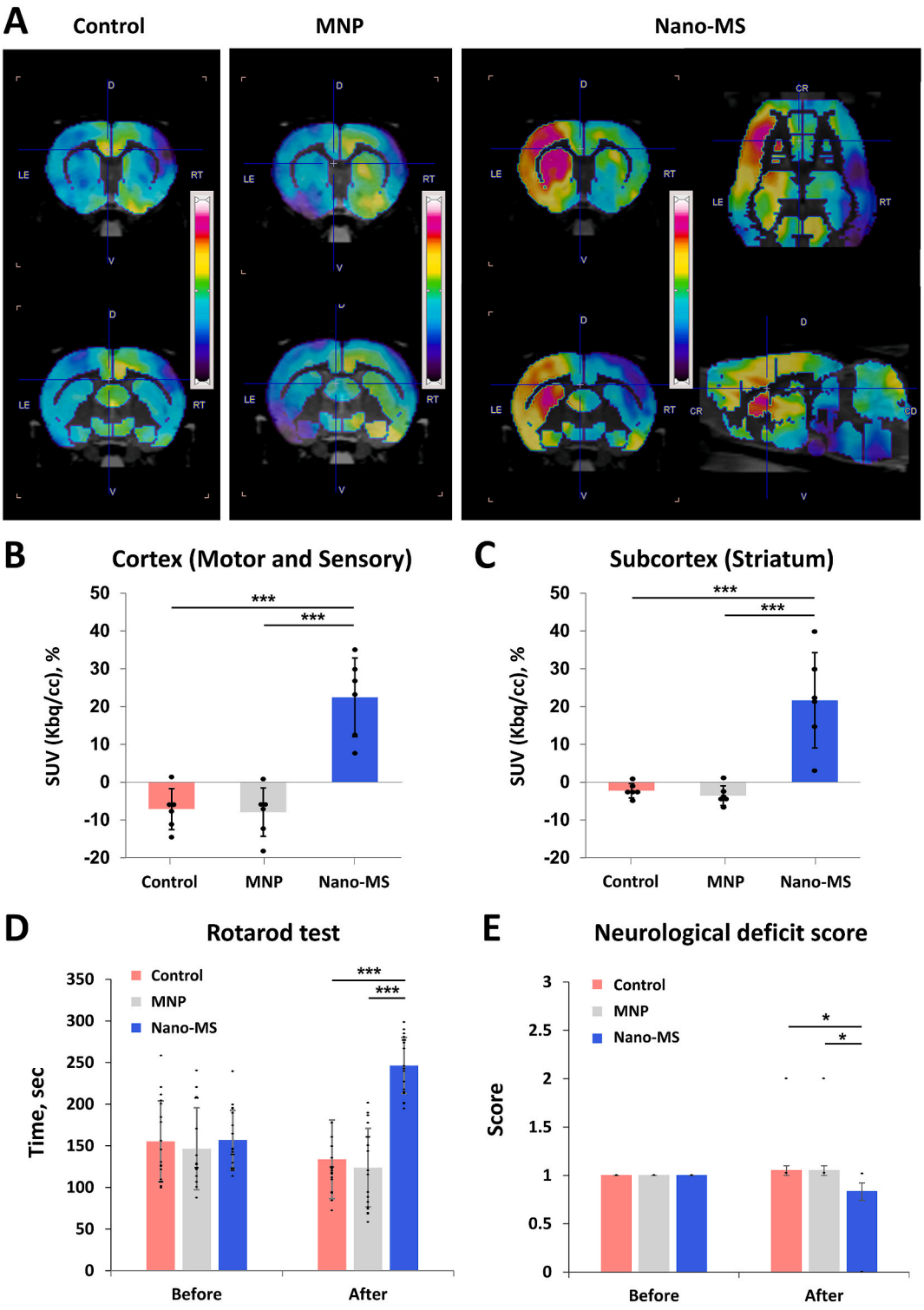

Fig. 3. Brain PET imaging and motor function. (A) In vivo brain FDG PET images illustrate metabolic changes post-treatment. The magnetic stimulation (Nano-MS) group displayed a notable increase in metabolic activity in both the (B) cortex and (C) subcortex compared to the Control and MNP groups. The motor function changes from baseline after treatment were evident by (D) a rotarod test and (E) the neurological deficit score. Repeated-measures ANOVA for the rotarod test showed a significant interaction between treatment and time ($p < 0.001$) with the main effect of treatment ($p < 0.001$). Significantly longer times to fall were observed in the Nano-MS group compared to the Control ($p < 0.001$) and MNP ($p < 0.001$) groups in post hoc analysis using Tukey's test. The data are shown as the mean ± standard deviation (n = 6 in each group). *: $p < 0.05$, **: $p < 0.01$, ***: $p < 0.001$.

3.3. Functional recovery of ischemic stroke

We performed rotarod tests to assess the restoration of motor function in subacute stroke following Nano-MS therapy. These tests measure coordination, balance, and endurance in animals subjected to focal ischemic injury throughout their post-treatment recovery [21]. The rotarod test offers a more precise evaluation of significant motor function impairments compared to beam walking and balance tests [22].

Fig. 3 presents the average time until fall and the variations in the rotarod tests for each group. Before treatment, the time until fall was similar across the three experimental groups. However, post-treatment times to fall (seconds ± SD) in the Nano-MS (246.5 ± 33.7) group was longer than those in the Control (133.7 ± 47.2) and MNP (123.7 ± 47.1) groups (treatment × time interaction effect, $F_{2,51} = 19.332$, $p < 0.001$; main effect of time, $F_{1,51} = 3.203$; $p = 0.079$; main effect of treatment, $F_{2,51} = 23.633$, $p < 0.001$; two-way ANOVA for repeated measures), suggesting enhanced balance and endurance for the Nano-MS group ($p < 0.001$ compared to the Control group, $p < 0.001$ compared to the MNP group, Tukey's post hoc analysis; **eTable II)**. Additionally, the improvement rate of neurological deficit scores for the Nano-MS group was higher (16.7 %) than those for the Control and MNP groups (−5.6 %) following treatment (Fig. 3 and eTable II).

3.4. Nano-MS ameliorates neuronal hyperexcitability in MCAO

We examined the effect of Nano-MS on intrinsic firing characteristics of motor cortical neurons in MCAO rats via whole-cell patch clamp recordings from the second and third layer pyramidal neurons in the primary motor cortex of the ischemic hemisphere (Fig. 1). We recorded pyramidal cells' voltage responses, elicited by current step pulses from −100 to 400 pA in 50 pA increments, and compared the intrinsic firing properties between groups.

Fig. 4A illustrates that pyramidal neurons in all groups exhibited tonic firing patterns with slight spike adaptation upon intracellular injection of the depolarizing current. We compared the excitability in each group by plotting the relationship curve between current injection intensity and firing frequency (Fig. 4B). Fig. 4C presents the gain, defined as the slope of the frequency-current intensity (f–I) curve and indicative of neuronal intrinsic excitability. The average gain value in the Control group was double that of the Sham group. Nano-MS therapy reduced this

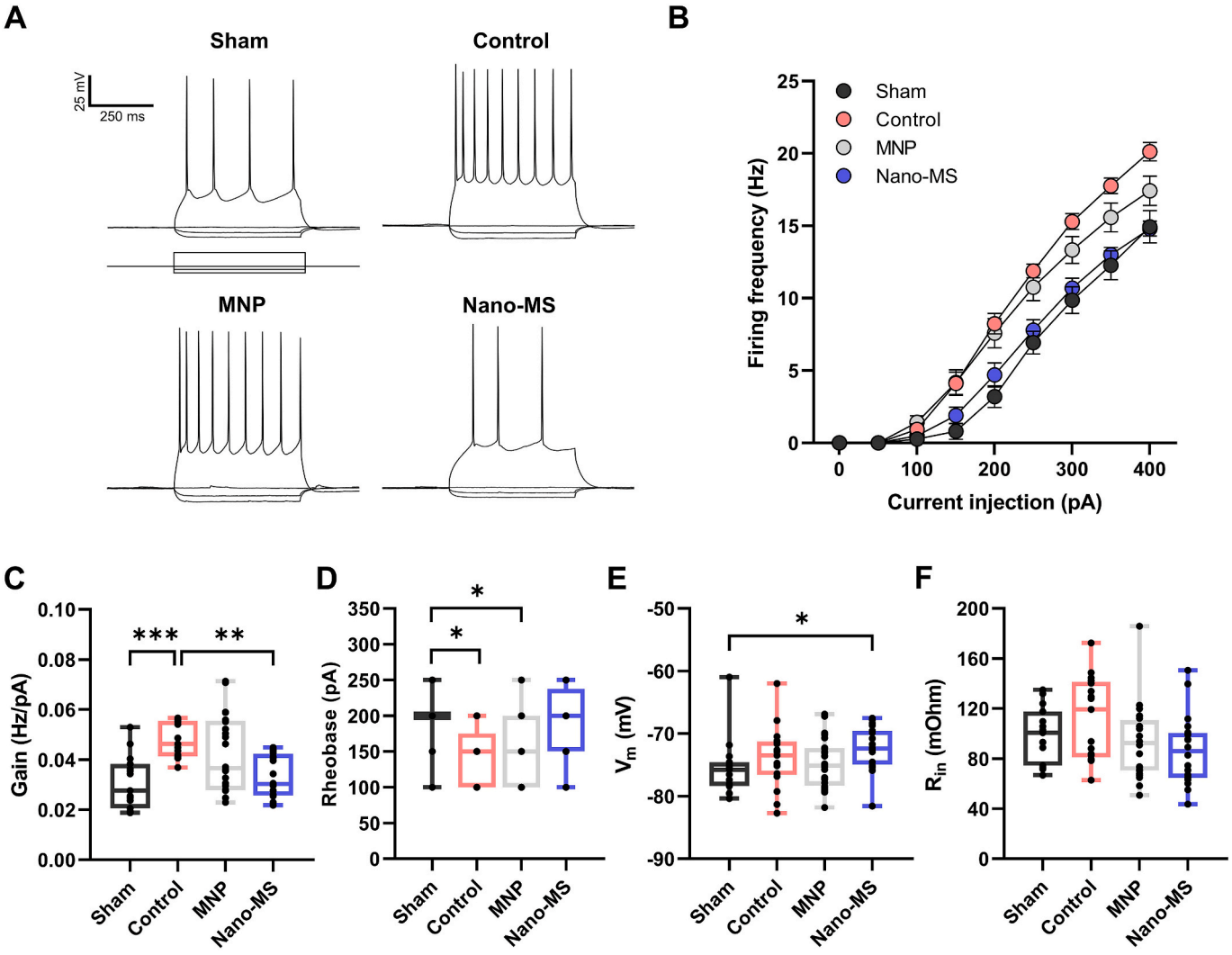

Fig. 4. Electrophysiology of pyramidal neurons in motor cortex layer 2–3. (A) Representative traces of membrane potential in each group, induced by 500-ms current pulses at −100, −50, 0, and 300 pA. (B) The correlation between current injection intensity and firing frequency (f-I curve). (C) Group average values of the f-I curve gain (Sham: 0.028 [0.021; 0.038]; Control: 0.046 [0.041; 0.056]; MNP: 0.037 [0.028; 0.056]; Nano-MS: 0.030 [0.026; 0.042]; unit: Hz/pA). (D) Group average values of rheobase (Sham: 200 [200; 200]; Control: 150 [100; 175]; MNP: 150 [100; 200]; Nano-MS: 200 [150; 238]; unit: pA). (E) Group average values of the resting membrane potential (Sham: 76.2 [-78.7;-74.7]; Control: 73.5 [-76.6;-71.3]; MNP: 75.1 [-78.3;-72.3]; Nano-MS: 72.4 [-75.0;-69.6]; unit: mV). (F) Group average values of input resistance (Sham: 101 [74.6; 118]; Control: 119 [81.1; 141]; MNP: 92.3 [70.5; 111]; Nano-MS: 86.0 [64.7; 100]; unit: MΩ). A single brain slice was prepared per animal. The number of recorded neurons is indicated beneath each bar (n = 4, 7, 8, and 6 for Sham, Control, MNP, and Nano-MS, respectively). All data were analyzed using the Kruskal-Wallis test with Dunn's post hoc analysis (median with interquartile range indicating min to max whiskers of box plots). *: $p < 0.05$, **: $p < 0.01$, ***: $p < 0.001$.

value to levels comparable to the Sham group (Sham: 0.028 [0.021; 0.038]; Control: 0.046 [0.041; 0.056]; MNP: 0.037 [0.028; 0.056]; Nano-MS: 0.030 [0.026; 0.042]; unit: Hz/pA; Kruskal–Wallis test, $p < 0.001$, **eTable III**).

To investigate the detailed mechanisms by which Nano-MS rescued the increased gain shown in MCAO rats, we examined passive and active electrophysiological properties of depolarizing current-evoked APs in each group. The rheobase was significantly lower in the Control and MNP groups compared with the Sham group (Sham: 200 [200; 200]; Control: 150 [100; 175]; MNP: 150 [100; 200]; Nano-MS: 200 [150; 238]; unit: pA; Kruskal–Wallis test, $p = 0.004$; Fig. 4D). No significant difference was found between the Nano-MS and Control groups ($p = 0.116$, **eTable IV)**. Nano-MS therapy led to a depolarization of the resting membrane potential relative to the Sham group (Sham: 75.8 [−78.4;-74.6]; Control: 73.5 [−76.6;-71.3]; MNP: 75.1 [−78.3;-72.3]; Nano-MS: 72.4 [−75.0;-69.6]; unit: mV; Kruskal–Wallis test, $p = 0.024$; Fig. 4E and eTable V). No significant differences were observed in input resistance (Fig. 4F and eTable VI).

As shown in Fig. 5, the Nano-MS group showed a significantly depolarized AP threshold compared to the Control group (Sham: −39.7 ± 1.0 mV, Control: 36.9 ± 1.1 mV, MNP: −38.2 ± 1.0 mV, Nano-MS: −32.5 ± 0.9 mV; one-way ANOVA, $p < 0.0001$; **eTable VII**). The AHP amplitudes were comparable among the groups **(eTable VIII).** However, AHP analysis revealed that AHP duration in the Control group was significantly reduced compared to the Sham group, and Nano-MS significantly increased AHP duration equivalent to the Sham group (Sham: 70.0 [56.7; 101]; Control: 54.3 [38.8; 53.4]; MNP: 57.7 [41.3; 85.0]; Nano-MS: 70.8 [53.3; 83.6]; unit: ms; Kruskal–Wallis test, $p = 0.001$; **eTable IX**). We compared the AHP slope for each group, defined as a linear slope of AHP amplitude within a 20–60 % interval, to exclude the possibility that alteration of the AP threshold may affect AHP duration [18]. The AHP slope for the Nano-MS group was significantly lower than that for the Control group (Sham: 0.208 ± 0.022 mV/ms, Control: 0.269 ± 0.012 mV/ms, NMP: 0.256 ± 0.018 mV/ms, Nano-MS: 0.198 ± 0.014 mV/ms, one-way ANOVA, $p < 0.01$; **eTable X**).

3.5. qRT-PCR for neuroinflammatory markers

We evaluated the expression levels of proinflammatory factors and adhesion molecules to quantify gene expression levels following therapy. As shown in Fig. 6, the expression of inflammatory cytokines and chemokines such as IL-1β, IL-6, TNF-α, and MCP-1 in the Nano-MS group were significantly reduced post-treatment compared to the Control and MNP groups. Furthermore, adhesion molecule markers, such as ICAM-1, exhibited elevated gene expression across the three MCAO groups, with a notable reduction following Nano-MS therapy (**eTable II**).

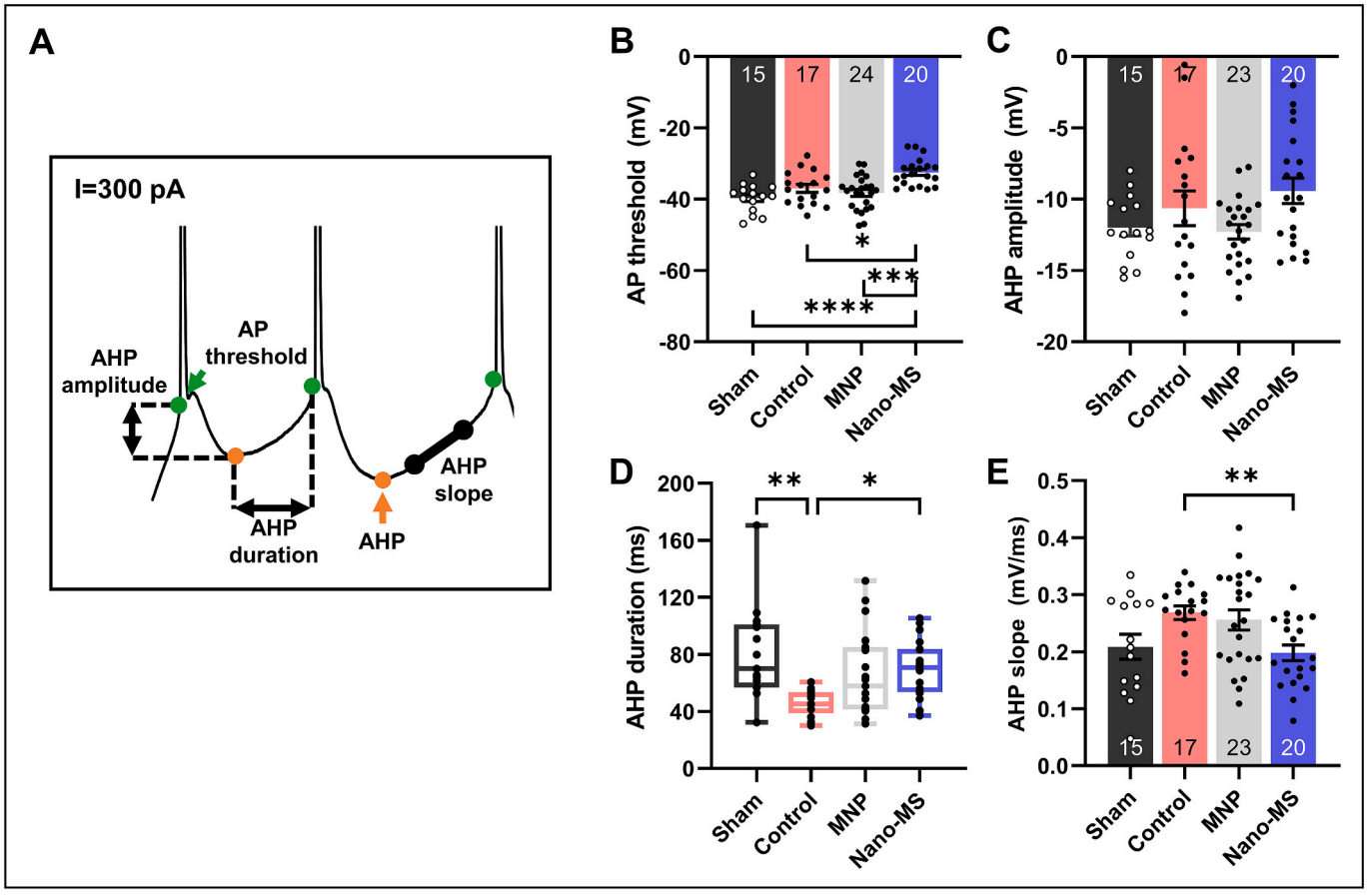

Fig. 5. Analysis of repetitive action potential (AP) trace at a 300 pA injected current. (A) A diagram explaining the analysis of active membrane properties. We measured AP threshold, afterhyperpolarization (AHP) amplitude, AHP duration, and AHP slope from the trace. (B) Group average values of the AP threshold (Sham: −39.7 ± 1.0 mV; Control: −36.9 ± 1.1 mV; MNP: −38.2 ± 1.0 mV; Nano-MS: −32.5 ± 0.9 mV). (C) Group average values of the AHP amplitude (Sham: −12.0 ± 0.6 mV; Control: −10.6 ± 1.2 mV; MNP: −12.3 ± 0.5 mV; Nano-MS: −9.4 ± 0.9 mV). (D) Group average values of the AHP duration (Sham: 70.0 [56.7; 101]; Control: 54.3 [38.8; 53.4]; MNP: 57.7 [41.3; 85.0]; Nano-MS: 70.8 [53.3; 83.6]; unit: ms). (E) Group average values of the AHP slope (Sham: 0.208 ± 0.022 mV/ms; Control: 0.269 ± 0.012 mV/ms; NMP: 0.256 ± 0.018 mV/ms; Nano-MS: 0.198 ± 0.014 mV/ms). We prepared a single brain slice per animal. The number of recorded neurons is indicated beneath each bar (n = 4, 7, 8, and 6 for Sham, Control, MNP, and Nano-MS, respectively). Parametric data presented as the mean ± standard error of mean. Nonparametric data are presented as the median with interquartile range indicating min to max whiskers of box plots. *: $p < 0.05$, ***: $p < 0.001$, ****: $p < 0.0001$.

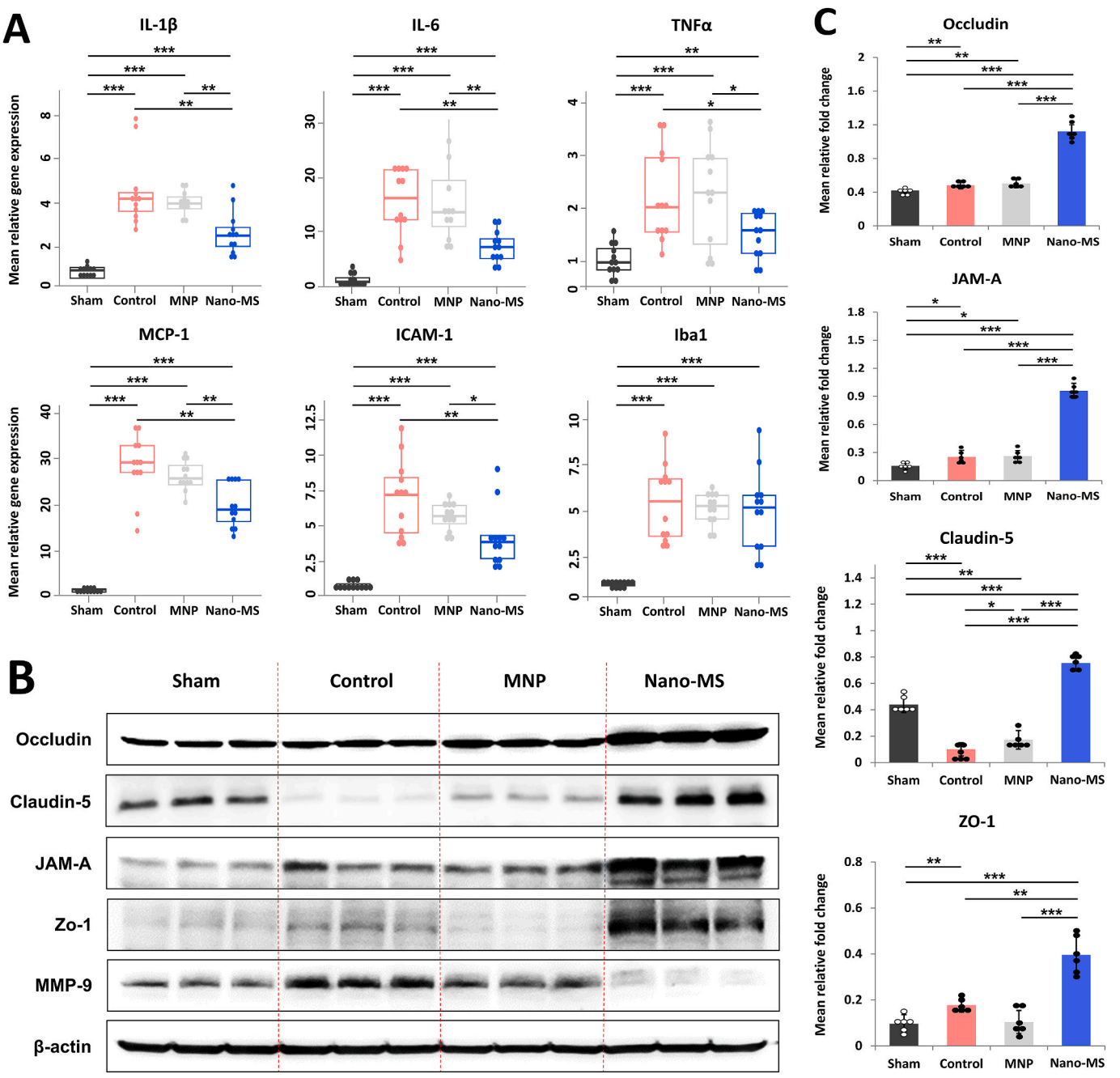

Fig. 6. RT-PCR and immunoblot analysis. (A) RNA isolation and RT-PCR for IL-1 beta, IL-6, TNF-alpha, MCP-1, ICAM-1, and Iba-1 mRNA expression levels. (B) Immunoblot analysis for protein expression. We used Western blot analysis (C) to determine protein expression levels of occludin, JAM-A, claudin-5, and ZO-1. Nonparametric data are presented as the median with interquartile range indicating min to max whiskers of box plots. Parametric data presented as the mean ± standard deviation (n = 6 in each group). *: $p < 0.05$, **: $p < 0.01$, ***: $p < 0.001$.

3.6. Immunoblot analysis for tight junction proteins

To investigate the effect of Nano-MS on tight junction protein expression, we evaluated the protein levels of claudin-5, occludin, ZO-1, and JAM-A (Fig. 6). The expression of tight junction protein levels was significantly higher in the Nano-MS group than in the Control and MNP groups, enhancing BBB integrity via the restoration of endothelial function. In the Nano-MS group, MMP-9 activity was significantly diminished relative to the Control and MNP groups, which correlates with reduced excitotoxicity and BBB disruption (Fig. 7). Regarding BBB permeability, Nano-MS treatment led to the upregulation of tight junction protein expression and a decrease in MMP-9 activity in MCAO rats (**eTable II**).

3.7. Immunofluorescence for apoptosis and neurogenesis

We quantified CC3/NeuN-positive cells to assess apoptotic activity in the boundary area of cerebral ischemia (Fig. 7). The incidence of CC3/NeuN-positive apoptotic cells was notably higher in the Control (26.3 ± 5.2) and MNP (22.7 ± 5.9) groups than in the Sham (1.1 ± 0.5) group (**eTable II**). However, these cells were significantly less prevalent in the Nano-MS (2.0 ± 1.0) group compared to the Control and MNP groups. To evaluate endogenous neurogenesis in the boundary area of the cerebral ischemia, we examined the presence of BrdU-positive cells in the perilesional frontal cortex near the subventricular zone. BrdU/NeuN and BrdU/DCX-positive cells were scarcely observed in the Control (1.2 ± 0.5, 3.2 ± 0.6) and MNP (2.3 ± 0.6, 2.7 ± 0.3) groups. Conversely, in

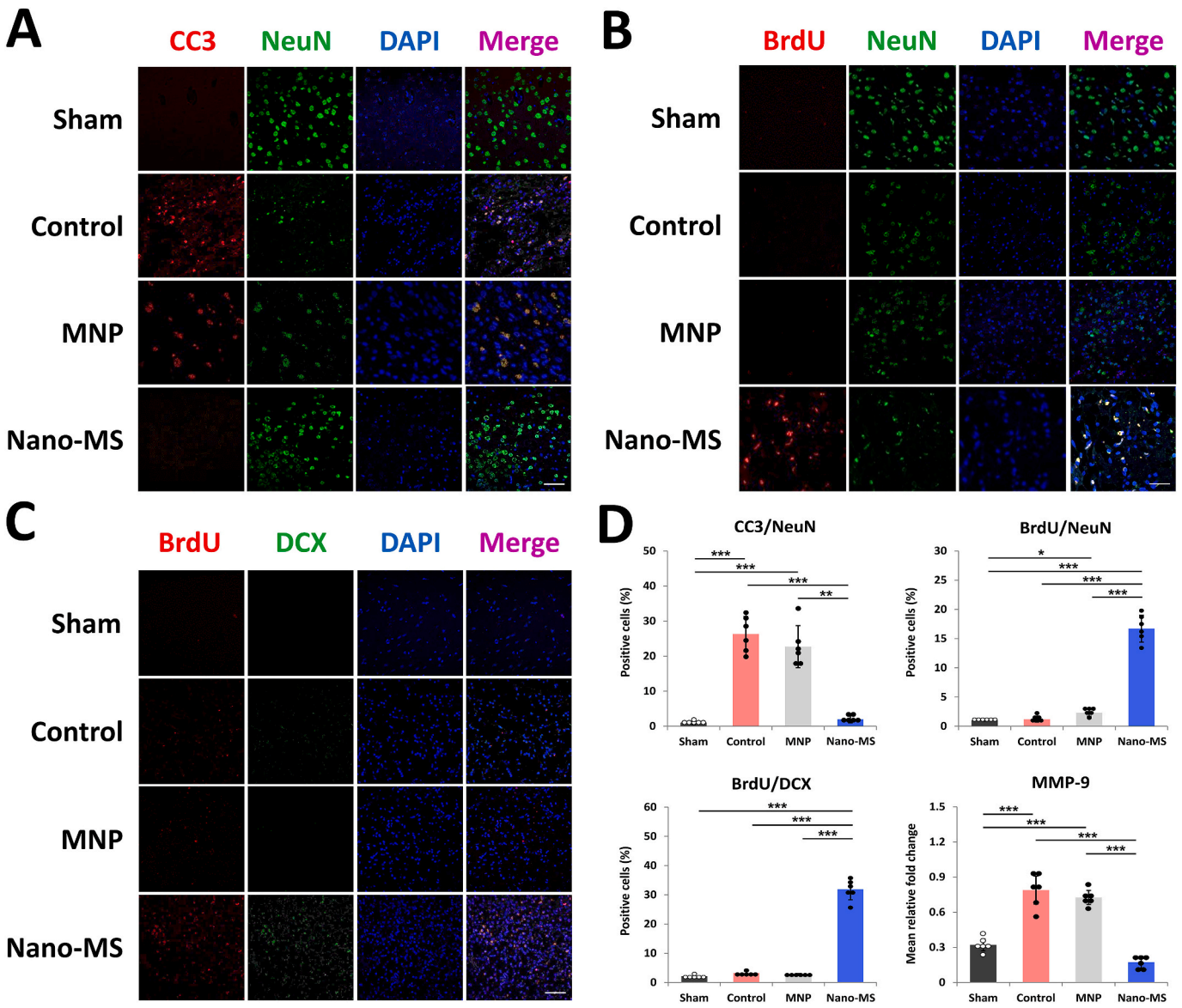

Fig. 7. Representative confocal images of the ischemic penumbra in the frontal cortex. (A) Staining for cleaved caspase-3 (CC3; red) and NeuN (green). (B) Staining for BrdU (red) and NeuN (green). (C) Staining for BrdU (red) and doublecortin (DCX; green). (D) Quantitative analysis of CC3 and NeuN colocalization (D1), BrdU and NeuN colocalization (D2), BrdU and DCX colocalization (D3), and MMP-9 expression levels (D4). Data are presented as the mean ± standard deviation (n = 6 in each group; Scale bar of 50 μm; 200x magnification). *: $p < 0.05$, **: $p < 0.01$, ***: $p < 0.001$. (For interpretation of the references to colour in this figure legend, the reader is referred to the Web version of this article.)

the Nano-MS group, BrdU/NeuN (16.7 ± 2.3) and BrdU/DCX-positive cells (31.9 ± 3.6) were profusely present in the penumbra (Fig. 7 and eTable II).

3.8. Evans blue staining and fluorescence imaging

To determine the safety of Nano-MS therapy, we analyzed fluorescence imaging with Evans blue. In the Nano-MS group, no Evans blue leakage was observed within the infarct area at the level observed when there was BBB disruption in our prior proof-of-concept study, other than the artifact (**eFigure II**) [10].

4. Discussion

Our study demonstrates that focused Nano-MS therapy alleviates post-stroke motor deficits and metabolic inactivity in subacute MCAO rats. Nano-MS therapy reduced hyperexcitability and neuroinflammation and improved endothelial function, BBB stabilization, and neurogenesis. Our results suggest that targeted, focused Nano-MS therapy to the motor cortex could be a promising and innovative noninvasive treatment for chronic ischemic motor deficits. These results are of potential clinical significance as motor deficits are the most significant residual impairments in patients with ischemic stroke.

Our prior proof-of-concept study showed that our focused Nano-MS therapy effectively and non-invasively stimulates brain regions with the highest precision [10]. The stimulation range of Nano-MS is approximately 3.5 mm. Although invasive approaches have been extensively investigated in animal models, recent endeavors are directed toward noninvasive techniques in clinical settings [2,3,7–9]. Magnetic stimulation strategies have been used to alter intrinsic neuronal plasticity [23,24], a potential therapeutic target for stroke [25]. Unlike the current rTMS and tDCS, which are limited by deep brain penetration and precise localization, the advantage of focused Nano-MS therapy lies in its ability to adjust the magnetic field's gradient force, achieving sustained and

precise stimulation in the targeted area to non-invasively restore brain function [4]. Additionally, focused Nano-MS can access deep brain structures, indicating its promise in improving chronic post-stroke motor function.

We used a systemic injection to ensure that Nano-MS is safe and clinically applicable. Previous studies used the stereotactic direct injection method for magnetothermal stimulation [26,27]. However, intralesional infusion is challenging to apply in the real-world clinical setting and poses a risk of surgery and infection. MNPs can be stuck to the blood vessel wall due to the non-zero gradient magnetic field in the FFP region. Nano-MS can provide focused stimulation to a targeted area. The MNPs we utilized have a blood circulation half-life of 37 min, and previous studies conducted in the same manner demonstrate that MNPs are in the brain capillaries 30 min after injection [11,28]. Therefore, we treated the rats using Nano-MS for 30 min post-MNP injection. MNPs can be cleared within 4 days in the body [29], and our prior study showed that the effect of MNPs disappeared after 48–72 h [10]. Therefore, we developed a safe and convenient twice-weekly treatment method. IA could be ten times more effective in target brain delivery than IV at the first Nano-MS stimulus [30–32]. Progressive development of clinically applicable methods and theranostic platforms combining diagnostic and therapeutic approaches is ongoing [33].

Focused Nano-MS therapy reduces motor impairment and enhances motor function in ischemic animal models from the subacute to the chronic stage. Nano-MS may ameliorate neurological motor dysfunction by modulating the abnormal hyperexcitability of the targeted layer 2/3 neurons in the motor cortex by regulating electrophysiological AP and AHP characteristics in pyramidal neurons during subacute cortical ischemia. Neuronal excitability in motor cortical neurons of the affected hemisphere in MCAO rats was identified using whole-cell patch clamp techniques. Despite its depolarizing effect on resting membrane potentials, focused Nano-MS therapy normalized abnormal excessive neuronal excitability by adjusting the after-hyperpolarization of the action potential in motor cortical neurons. Focused Nano-MS significantly depolarized the AP threshold for spike initiation in the targeted layer 2/3 motor cortex. Nano-MS also prolonged the AHP duration and reduced the AHP slope, effectively spacing AP firing in the pyramidal neurons of the targeted layer 2/3 primary motor cortex. The Nano-MS-induced modulation of AHP might reduce the hyperexcitability of the layer 2/3 primary motor cortex by curtailing the increased AP firing frequency in MCAO rats. However, Nano-MS therapy did tend to increase but failed to demonstrate a statistically significant impact on the rheobase compared with the Control group. Further study is needed to determine this discrepancy, likely due to large current steps (50 pA) applied to evoke AP.

Regarding the electrophysiological mechanisms, temperature changes within the central nervous system have a broad effect on neuronal function through alterations in receptor kinetics, channel conductances, and synaptic transmission, which can lead to neuroplasticity [34]. Previous research has demonstrated that hyperthermia at 39 °C reduces excitatory neurotransmission in cultured hippocampal neurons and that a physiological temperature increase diminishes evoked field potentials in rat frontal cortex brain slices. The latter is affected by the temperature-dependent shift in the balance of excitatory and inhibitory inputs [35,36]. In line with these findings, we induced brain hyperthermia using focused Nano-MS directed at the primary motor cortex, which mitigated the neuronal excitability observed from the subacute to the chronic phases of ischemic stroke.

Our results suggest that Nano-MS-induced hyperthermia may facilitate neuroplasticity and promote functional recovery in subacute ischemia. Tissue temperature changes by magnetothermal stimulation using MNPs can directly modulate neuronal activity through various thermo-sensitive ion channels, including TRP channels. Recent research indicates that targeted stimulation of the TRPV1 channel can modulate the activity of specific brain regions, thus regulating neuroplasticity by safely raising tissue temperature [26,27]. We demonstrated that Nano-MS could induce hyperthermia sufficiently and activate neurons via TRPV1 channels in the primary motor cortex [37]. To verify the effect of Nano-MS on neural activation via stimulation of the TRPV1 channel, we tested whether a TRPV1 antagonist could block this activity by Nano-MS using c-fos staining. Consequently, the TRPV1 antagonist blocked Nano-MS-induced neuronal activation. These results suggest that the effects of Nano-MS are mediated at least partially via TRPV1 channel activation, a well-documented method of increasing neuroplasticity. However, the characteristics of TRPV1 expression may differ between rodents and humans [38,39]. More research is needed to extrapolate the results from our models into outcomes for human patients with stroke.

Improvements in post-stroke motor function induced by Nano-MS are attributed to suppressing the inflammatory response following ischemic injury and enhancing brain metabolic function. Significant enhancements in neuroinflammation, BBB integrity, apoptosis, neurogenesis, and metabolic activity were observed following Nano-MS therapy. These findings align with the pathophysiological mechanisms of cerebral ischemia, where inflammatory factors can initiate or amplify inflammation, exacerbate ischemic damage, and trigger a series of pathological cascades, including neuronal cell apoptosis/death and BBB compromise. This culminates in neuronal dysfunction [40]. FDG PET imaging supports the positive impact of targeted Nano-MS therapy on ischemic lesions. The reduced metabolism in stroke lesions is indicative of diminished neuronal activity [41]. Notably, brain glucose metabolism in both the cortex and subcortex was significantly increased, by approximately 20 %, in the Nano-MS group, and decreased in the Control and MNP groups. These results suggest an improvement in brain metabolic function for the Nano-MS group. Increased glucose uptake might be misinterpreted as worsening neuroinflammation post-stroke [42]. However, the diminished expression of inflammatory cytokines in the Nano-MS group likely clarifies that the observed hypermetabolism in the cortex and subcortex results from enhanced brain metabolic function rather than neuroinflammation.

Nano-MS therapy may restore functional activity by stabilizing the BBB, diminishing apoptosis, and promoting neurogenesis via the modulation of abnormal hyperexcitability and attenuation of neuroinflammation in the ischemic penumbra. While the ischemic core results in instantaneous cell death, the penumbra, the surrounding area of the ischemic core, comprises potentially-reversible call injury [43]. Previous studies employing the MCAO model indicate that the penumbra region experiences a significant downregulation of gamma-aminobutyric acid (GABA) receptors, a decrease in GABA current, heightened intrinsic neuronal excitability, and an increase in the probability of presynaptic glutamate neurotransmitter release [8,9]. Therefore, numerous therapeutic strategies have been explored to reverse the aberrant brain activity following an ischemic stroke [2,3,8,9,44]. Additionally, extensive evidence suggests that targeting neuroinflammation may offer neuroprotection in the ischemic penumbra [45]. Our data support that regulating excessive brain activity and neuroinflammation with Nano-MS could enhance post-stroke motor recovery by preventing further cell death in the peri-infarct area.

This study has several limitations. First, as our study demonstrated a treatment effect for only one week, caution must be exercised when considering the implications for long-term post-stroke motor rehabilitation and functional restoration of neuronal circuits by neurogenesis with Nano-MS. Extended research on the optimal Nano-MS therapy protocol is warranted. Second, the interpretation of electrophysiological data is constrained to the firing patterns and AP measurements obtained from layer 2/3 excitatory neurons in the rat motor cortex. Further investigation is required to elucidate the impact of Nano-MS therapy on the firing properties and ion channels of various cell types, including inhibitory interneurons and glia, across all cortical layers. Additionally, the number of animals in each electrophysiological group was unbalanced. We prepared more animals in the MCAO group, anticipating a higher failure rate of whole-cell patch-clamp recordings due to MCAO-

induced ischemic cortical injury. However, since the recordings proceeded successfully in all groups, including the MCAO rats, and all recording data were included in the analysis to avoid selection bias, the animal numbers of each group were unintentionally unbalanced. This imbalance could influence statistical results and compromise data representativeness due to potential sampling bias, thus necessitating cautious interpretation and further studies with balanced sample sizes to generalize the findings. Moreover, access resistance was not continuously monitored throughout the recordings. An increase in access resistance during recording, as the neuronal membrane reseals, could affect the accuracy of membrane potential measurements in current-clamp mode, particularly by broadening AP duration and reducing AP amplitude [46]. It may also lead to an artificial decrease in gain, an increase in rheobase, and depolarization of the AP threshold. Therefore, future studies should exclude cells with a drift in access resistance to ensure accurate measurements. Third, since this study was conducted on young animals, further investigation is necessary to evaluate its applicability to human adult patients. Fourth, our experimental groups did not include the magnetic stimulation group without MNPs. Previous studies reported no stimulus delivery with the magnetic field without MNPs [11,27]. However, the results for this group may be significant, and further studies are needed to examine the impact of magnetic stimulation without MNPs. Lastly, anesthesia may confound the effect of Nano-MS, as rTMS outcomes are reported to differ between anesthetized and awake animals [47]. Thus, further investigation evaluating the impact of anesthesia on Nano-MS is necessary.

5. Conclusion

In summary, this study presents the beneficial effects of focused Nano-MS for recovering motor behavioral deficits and brain metabolic inactivity in subacute ischemic stroke. This is the first study to demonstrate that focused Nano-MS therapy can improve neuronal excitability, neuroinflammation, BBB stabilization, and neurogenesis. Our findings support the feasibility of focused Nano-MS therapy as a promising, innovative, noninvasive treatment for patients with post-stroke motor deficits. Further research is warranted.

Sources of funding

This work was supported by a National Research Foundation (NRF) of Korea Grant funded by the Korean Government (2023R1A2C2006414, 2021M3C1B8036779, and 2019M3C1B8090798) and the Korea Evaluation Institute of Industrial Technology (KEIT 20003822).

Ethics approval and consent to participate

All protocols adhered to the Chonnam National University guidelines for the care and use of laboratory animals and were approved by the Institutional Animal Care and Use Committee. The study complied with the National Institutes of Health guidelines concerning the care and use of animals in experimental procedures.

Availability of data and materials

The data that support the findings of the current study are available from the corresponding author on reasonable request.

CRediT authorship contribution statement

Ja-Hae Kim: Writing – original draft, Supervision, Investigation, Formal analysis, Data curation. **Minhee Jeong:** Writing – original draft, Investigation, Formal analysis, Data curation. **Hohyeon Kim:** Writing – original draft, Methodology, Investigation. **Ji-Hye Kim:** Methodology, Investigation, Formal analysis, Data curation. **Ji Woong Ahn:** Supervision, Investigation. **Boyoung Son:** Resources. **Kang-Ho Choi:** Writing – review & editing, Validation, Supervision, Resources, Methodology, Investigation, Funding acquisition, Formal analysis, Data curation, Conceptualization. **Seungsoo Chung:** Writing – review & editing, Supervision, Investigation, Formal analysis. **Jungwon Yoon:** Writing – review & editing, Supervision, Methodology, Investigation, Data curation, Conceptualization.

Declaration of competing interest

The authors declare that they have no known competing financial interests or personal relationships that could have appeared to influence the work reported in this paper.

Acknowledgments

None.

Appendix A. Supplementary data

Supplementary data to this article can be found online at https://doi.org/10.1016/j.brs.2024.08.011.

Abbreviations

rTMS = repetitive transcranial magnetic stimulation
tDCS = transcranial direct current stimulation
Nano-MS = magnetothermal brain stimulation using magnetic nanoparticles
FFP = field-free point
BBB = blood-brain barrier
SD = Sprague-Dawley
MCAO = middle cerebral artery occlusion
MNP = magnetic nanoparticles
MNPO = magnetic nanoparticles occlusion
NDS = neurological deficit score
AP = action potentials
AHP = afterhyperpolarization
IL = interleukin
TNF-α = tumor necrosis factor-alpha
MCP-1 = monocyte chemoattractant protein-1
ICAM-1 = intercellular adhesion molecule-1
TRPV1 = transient receptor potential (TRP) vanilloid-1

References

[1] Tsao CW, Aday AW, Almarzooq ZI, et al. Heart disease and stroke statistics-2022 update: a report from the American heart association. Circulation 2022;145:e153–639.
[2] Edwards DJ, Liu CY, Dunning K, et al. Electric field navigated 1-Hz rTMS for poststroke motor recovery: the E-FIT randomized controlled trial. Stroke 2023;54:2254–64.
[3] Baker KB, Plow EB, Nagel S, et al. Cerebellar deep brain stimulation for chronic post-stroke motor rehabilitation: a phase I trial. Nat Med 2023;29:2366–74.
[4] Li KP, Wu JJ, Zhou ZL, et al. Noninvasive brain stimulation for neurorehabilitation in post-stroke patients. Brain Sci 2023;13.
[5] Carmichael ST. Brain excitability in stroke: the yin and yang of stroke progression. Arch Neurol 2012;69:161–7.
[6] Huynh W, Vucic S, Krishnan AV, Lin CS, Kiernan MC. Exploring the evolution of cortical excitability following acute stroke. Neurorehabilitation Neural Repair 2016;30:244–57.
[7] Badoiu A, Mitran SI, Catalin B, et al. From molecule to patient rehabilitation: the impact of transcranial direct current stimulation and magnetic stimulation on stroke-A narrative review. Neural Plast 2023;2023:5044065.
[8] Bitar L, Uphaus T, Thalman C, et al. Inhibition of the enzyme autotaxin reduces cortical excitability and ameliorates the outcome in stroke. Sci Transl Med 2022;14:eabk0135.
[9] Hleihil M, Vaas M, Bhat MA, Balakrishnan K, Benke D. Sustained baclofen-induced activation of GABA (B) receptors after cerebral ischemia restores receptor expression and function and limits progressing loss of neurons. Front Mol Neurosci 2021;14:726133.

[10] Kim H, Kim J, Kim J, Oh S, Choi K, Yoon J. Magnetothermal-based non-invasive focused magnetic stimulation for functional recovery in chronic stroke treatment. Sci Rep 2023;13:4988.
[11] Tabatabaei SN, Girouard H, Carret AS, Martel S. Remote control of the permeability of the blood-brain barrier by magnetic heating of nanoparticles: a proof of concept for brain drug delivery. J Contr Release 2015;206:49–57.
[12] Koh SH, Park Y, Song CW, et al. The effect of PARP inhibitor on ischaemic cell death, its related inflammation and survival signals. Eur J Neurosci 2004;20:1461–72.
[13] Boroon MP, Ayani MB, Bazaz SR. Estimation of the optimum number and location of nanoparticle injections and the specific loss power for ideal hyperthermia. J Therm Biol 2018;72:127–36.
[14] Le TA, Bui MP, Yoon J. Theoretical analysis for wireless magnetothermal deep brain stimulation using commercial nanoparticles. Int J Mol Sci 2019;20.
[15] Longa EZ, Weinstein PR, Carlson S, Cummins R. Reversible middle cerebral artery occlusion without craniectomy in rats. Stroke 1989;20:84–91.
[16] Kida H, Tsuda Y, Ito N, et al. Motor training promotes both synaptic and intrinsic plasticity of layer II/III pyramidal neurons in the primary motor cortex. Cerebr Cortex 2016;26:3494–507.
[17] Nigro MJ, Hashikawa-Yamasaki Y, Rudy B. Diversity and connectivity of layer 5 somatostatin-expressing interneurons in the mouse barrel cortex. J Neurosci 2018;38:1622–33.
[18] Fourcaud-Trocme N, Zbili M, Duchamp-Viret P, Kuczewski N. Afterhyperpolarization promotes the firing of mitral cells through a voltage-dependent modification of action potential threshold. eNeuro 2022;9.
[19] Valenzano KJ, Grant ER, Wu G, et al. N-(4-tertiarybutylphenyl)-4-(3-chloropyridin-2-yl)tetrahydropyrazine -1(2H)-carbox-amide (BCTC), a novel, orally effective vanilloid receptor 1 antagonist with analgesic properties: I. in vitro characterization and pharmacokinetic properties. J Pharmacol Exp Therapeut 2003;306:377–86.
[20] De Winter JC. Using the Student's t-test with extremely small sample sizes. Practical Assess Res Eval 2019;18:10.
[21] Zarruk JG, Garcia-Yebenes I, Romera VG, et al. Neurological tests for functional outcome assessment in rodent models of ischaemic stroke. Rev Neurol 2011;53:607–18.
[22] Hamm RJ, Pike BR, O'Dell DM, Lyeth BG, Jenkins LW. The rotarod test: an evaluation of its effectiveness in assessing motor deficits following traumatic brain injury. J Neurotrauma 1994;11:187–96.
[23] Hoppenrath K, Hartig W, Funke K. Intermittent theta-burst transcranial magnetic stimulation alters electrical properties of fast-spiking neocortical interneurons in an age-dependent fashion. Front Neural Circ 2016;10:22.
[24] Tang AD, Hong I, Boddington LJ, et al. Low-intensity repetitive magnetic stimulation lowers action potential threshold and increases spike firing in layer 5 pyramidal neurons in vitro. Neuroscience 2016;335:64–71.
[25] King ES, Tang AD. Intrinsic plasticity mechanisms of repetitive transcranial magnetic stimulation. Neuroscientist 2024;30:260–74.
[26] Chen R, Romero G, Christiansen MG, Mohr A, Anikeeva P. Wireless magnetothermal deep brain stimulation. Science 2015;347:1477–80.
[27] Hescham SA, Chiang PH, Gregurec D, et al. Magnetothermal nanoparticle technology alleviates parkinsonian-like symptoms in mice. Nat Commun 2021;12:5569.
[28] Liu S, Chiu-Lam A, Rivera-Rodriguez A, et al. Long circulating tracer tailored for magnetic particle imaging. Nanotheranostics 2021;5:348–61.
[29] Park SJ, Han SR, Kang YH, et al. In vivo preclinical tumor-specific imaging of superparamagnetic iron oxide nanoparticles using magnetic particle imaging for cancer diagnosis. Int J Nanomed 2022;17:3711–22.
[30] Guzman R, Janowski M, Walczak P. Intra-arterial delivery of cell therapies for stroke. Stroke 2018;49:1075–82.
[31] Cooke JN, Ellis JA, Hossain S, Nguyen J, Bruce JN, Joshi S. Computational pharmacokinetic rationale for intra-arterial delivery to the brain. Drug Deliv Transl Res 2016;6:622–9.
[32] Pendharkar AV, Chua JY, Andres RH, et al. Biodistribution of neural stem cells after intravascular therapy for hypoxic-ischemia. Stroke 2010;41:2064–70.
[33] Buchholz O, Sajjamark K, Franke J, et al. In situ theranostic platform combining highly localized magnetic fluid hyperthermia, magnetic particle imaging, and thermometry in 3D. Theranostics 2024;14:324–40.
[34] Van Hook MJ. Temperature effects on synaptic transmission and neuronal function in the visual thalamus. PLoS One 2020;15:e0232451.
[35] Feng Z, Saha L, Dritsa C, Wan Q, Glebov OO. Temperature-dependent structural plasticity of hippocampal synapses. Front Cell Neurosci 2022;16:1009970.
[36] Gotoh M, Nagasaka K, Nakata M, Takashima I, Yamamoto S. Brain temperature alters contributions of excitatory and inhibitory inputs to evoked field potentials in the rat frontal cortex. Front Cell Neurosci 2020;14:593027.
[37] Han P, Korepanova AV, Vos MH, Moreland RB, Chiu ML, Faltynek CR. Quantification of TRPV1 protein levels in rat tissues to understand its physiological roles. J Mol Neurosci 2013;50:23–32.
[38] Lam PM, McDonald J, Lambert DG. Characterization and comparison of recombinant human and rat TRPV1 receptors: effects of exo- and endocannabinoids. Br J Anaesth 2005;94:649–56.
[39] Li T, Chung MK. Striving toward hyperthermia-free analgesia: lessons from loss-of-function mutations of human TRPV1. J Clin Invest 2023;133.
[40] Wu L, Xiong X, Wu X, et al. Targeting oxidative stress and inflammation to prevent ischemia-reperfusion injury. Front Mol Neurosci 2020;13:28.
[41] Heiss WD. The additional value of PET in the assessment of cerebral small vessel disease. J Nucl Med 2018;59:1660–4.
[42] Marchal G, Young AR, Baron JC. Early postischemic hyperperfusion: pathophysiologic insights from positron emission tomography. J Cerebr Blood Flow Metabol 1999;19:467–82.
[43] Fifield KE, Vanderluit JL. Rapid degeneration of neurons in the penumbra region following a small, focal ischemic stroke. Eur J Neurosci 2020;52:3196–214.
[44] Adhikari Y, Ma CG, Chai Z, Jin X. Preventing development of post-stroke hyperexcitability by optogenetic or pharmacological stimulation of cortical excitatory activity. Neurobiol Dis 2023;184:106233.
[45] Amantea D, Greco R, Micieli G, Bagetta G. Paradigm shift to neuroimmunomodulation for translational neuroprotection in stroke. Front Neurosci 2018;12:241.
[46] Petersen CCH. Whole-cell recording of neuronal membrane potential during behavior. Neuron 2017;95:1266–81.
[47] Gersner R, Kravetz E, Feil J, Pell G, Zangen A. Long-term effects of repetitive transcranial magnetic stimulation on markers for neuroplasticity: differential outcomes in anesthetized and awake animals. J Neurosci 2011;31:7521–6.